

Image Recognition of Breast Tumor Proliferation Level Based on Convolution Neural Network

Junhao Yang¹, Chunxiao Chen^{1,*}, Qingyang Zang¹ and Jianfei Li¹

Abstract: Pathological slide is increasingly applied in the diagnosis of breast tumors despite the issues of large amount of data, slow viewing and high subjectivity. To overcome these problems, a micrograph recognition method based on convolutional neural network is proposed for pathological slide of breast tumor. Combined with multi-channel threshold and watershed segmentation, a sample database including single cell, adhesive cell and invalid cell was established. Then, the convolution neural network with six layers is constructed, which has ability to classify the stained breast tumor cells with accuracy of more than 90%, and evaluate the proliferation level with relative error of less than 5%. The experimental result indicates the effectiveness of this approach, and is useful for providing an objective basis for evaluating the malignancy of breast tumors.

Keywords: Breast tumor, proliferation level, convolution neural network, immunohistochemical staining, pathological slide.

1 Introduction

In pathological diagnosis, the proliferation of tumors is an important basis to differentiate benign and malignant tumors and to suggest the prognosis of tumors [Friedman and Kim (2010); Atanassov, Mohan, Lan et al. (2016)]. Immunohistochemical staining based on the monoclonal antibody Ki-67 or proliferating cell nuclear antigen (PCNA) is able to distinguish cells in the division cycle and G0 phase cells from the tissue section to determine the proliferative capacity of the tumor and widely used in clinical diagnosis [Juríková, Danihel, Polák et al. (2016); Huang, Chen, Wang et al. (2016)]. The immunohistochemical stain classifies tumor cells based on different cell cycles according to the staining intensity. Accurate identification of cells in pathological sections is important for the diagnosis of tumors [Ikemura, Shibahara, Mukasa et al. (2016); Salomon, Köllerman, Thederan et al. (2008)].

At present, the interpretation method used in the diagnosis of clinical pathology is mainly manual viewing. This method relies on personal experience, and might draw a completely different conclusion by different doctors [Shui, Yu, Bi et al. (2016)]. In order to overcome the subjectivity of pathological diagnosis and to improve the efficiency and accuracy, Shete et al. [Shete and Kharate (2015)] combined thresholding of dyed intensity with watershed segmentation, and proposed an automatic detection method for breast cancer

¹ Department of Biomedical Engineering, Nanjing University of Aeronautics & Astronautics, Nanjing, 211106, China.

* Corresponding Author: Chunxiao Chen. Email: ccxbme@nuaa.edu.cn.

malignancy based on the proportion of dyeing area to the size of the whole image. Ko et al. [Ko, Chen and Lin (2016)] achieved the separation of overlapping nuclei by separating the stained regions on the basis of normalization of staining, which promoted the recognition accuracy of mammary tumor cells. For the identification and classification of suspected tumor cells in pathology, researchers have proposed many methods. Van Eycke et al. [Van Eycke, Allard, Salmon et al. (2017)] used color vector extraction and matching to solve the inter-assay differences of tonsil tumor immunohistochemical staining, and proposed a method to evaluate the necessity of image normalization, which has a certain increase in the recognition speed. Shi et al. [Shi, Zhong, Hong et al. (2016)] used an image processing method based on local correlation clustering to identify different types of cells for pathological slides of nasopharyngeal carcinoma, which overcomes the defects of low-quality images and improves the recognition accuracy. Fan et al. [Fan, Wei and Cao (2016)] used Back Propagation (BP) neural network based on feature extraction to extract the region of interest from lung cancer tissue section immunohistochemistry and optimized the extraction and segmentation of cancerous regions. In the study of pathological section target identification, most of the work starts with the classification of staining intensity based on the beliefs that the staining intensities of different types of cells are significantly different and the cells are relatively independent. Such beliefs in fact do not reflect the actual situation. Therefore, the related algorithms need to be improved with respect to the quantitative analysis of tumor cells.

Convolutional neural network is an efficient recognition algorithm widely used in pattern recognition, image processing and other fields in recent years. It has the characteristics of simple structure, less training parameters and strong adaptability. In view of the existing problems in the automatic identification of tumor cells in pathological slides of breast tumors, this paper proposes a method of image recognition for breast tumor cells based on convolutional neural network and calculates the tumor proliferation level, which is able to obtain relatively accurate diagnosis results.

2 Convolutional neural network

The structure of the Convolutional Neural Network (CNN) is a special multi-layer sensor, which is highly invariant to translation and other deformations, and therefore is particularly suitable for identifying two-dimensional shapes [Zbontar and LeCun (2016)]. CNN reduces the number of parameters mainly by two means. One is to use convolution to achieve local perception to reduce the number of parameters. The convolutional layer contains multiple feature maps, each of which represents certain aspect of the previous layer [Li, Tran, Thung et al. (2014)]. Pooling is another way of reducing the number of parameters by counting the average or maximum value of an image within a certain area to achieve downsampling. The subsampling of the upper layer by the pooling layer can reduce its complexity and prevent overfitting [Krizhevsky, Sutskever and Hinton (2012)]. In image applications, the convolutional neural network uses Stochastic Gradient Descent (SGD) and Graphics Processing Unit (GPU) to speed up the training process, which makes it more convenient to train large numbers of image data [Bottou (2010); Soos, Rak, Veres et al. (2008)]. In this study, we use the convolutional neural network to learn the characteristics of stained breast cancer cells in order to identify and classify them with

different differentiation abilities.

The convolutional neural network learns the characteristics of the original image through the cooperation of the convolutional layer and the pooling layer, and adjusts the parameters through the classic back propagation algorithm (BP) to achieve the update of the weights, and ultimately complete the learning task. The convolutional network structure uses a convolutional discrete type [LeCun, Bottou, Bengio et al. (1998)]. Expressed as

$$C_{(p,q)} = f\left(\sum_{i=1}^m \sum_{j=1}^n u_{(p+i-1,q+j-1)} * w_{(i,j)} + b_{(i,j)}\right) \quad (1)$$

where (p, q) is the coordinates of the pixel in the image, $u_{(p,q)}$ is the input data, $w_{(i,j)}$ is the weight matrix of the convolution kernel, $b_{(i,j)}$ is the offset of the convolution kernel, $m * n$ is the size of the convolution kernel and $f(\cdot)$ is the activation function.

The pooling layer samples the mapping features of the input. After sampling, the number of input features and output features remains the same, while the size of the output features will be significantly reduced compared to the size of the input characteristics. The pooling layer is represented as

$$u_{\beta}^{\gamma} = f(B_{\beta}^{\gamma} * sub(u_{\beta}^{\gamma-1}) + b_{\beta}^{\gamma}) \quad (2)$$

where γ is the number of network layers, β is a choice of input features, $sub(\cdot)$ represents the function used for subsampling, B_{β}^{γ} and b_{β}^{γ} are offsets of the output features. The meaning of $f(\cdot)$ is similar to that of the convolutional layer.

The learning target of CNN is to minimize the loss function $L(w, b)$, which typically adopts the mean squared error function, the cross-entropy cost function and the log-likelihood function. The derivative of the loss function for each layer is defined as the residual, and backpropagated by the gradient descent method. The training parameters w_t and b_t of the convolutional neural network are updated layer by layer [Li, Hao and Lei (2016)]. w_t and b_t denote the weights and offset vectors of the convolution kernel of the level t , and the learning rate η is used to control the strength of backward propagation of residuals.

$$w_t = w_t - \eta * \frac{\partial L(w, b)}{\partial w_t} \quad (3)$$

$$b_t = b_t - \eta * \frac{\partial L(w, b)}{\partial b_t} \quad (4)$$

In this study, we use the convolutional neural network to study the characteristics of the stained tumor cells to identify and classify the breast cancer cells with different differentiation abilities. To identify the proliferation level of one certain tissue section, it is necessary to extract independent cells from the original image, and add the counting weights according to the classification.

3 Methods

3.1 Mammary tumor proliferation level

Ki-67 is one of the essential biomarkers for assessment of proliferation rate in breast cancer screening and grading. Ki-67 image is shown in Fig. 1. The cells stained in dark brown were positive cells (P cells), i.e. tumor cells with strong proliferation ability; cells stained in blue were negative cells (N cell), corresponding to the G0 phase cells; the granular cells in the fibrous stroma were lymphocytes (L cells).

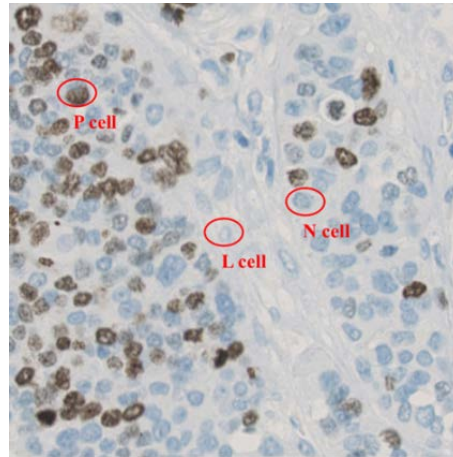


Figure 1: Beast tumor cells in Ki-67 image

Ki-67 positive index $Ki67_{index}$ can characterize the proliferation of tumors,

$$Ki67_{index} = \frac{Num_p}{Num_p + Num_N} \quad (5)$$

Where, Num_p is the number of positive cells and Num_N is the number of negative cells. Studies on breast tumors have shown that, Ki-67 positive rate below 2% indicates that the cell proliferation activity is low and the tumor can be diagnosed as benign; Ki-67 positive rate above 30% shows that the cell proliferation activity is extremely high and the tumor is highly malignant [Dowsett, Nielsen, A'Hern et al. (2011); Yang, Tang and Klimstra (2011); Shui, Yu, Bi et al. (2016); Focke, van Diest, Decker et al. (2016)].

3.2 Cell extraction

The automatic extraction and recognition algorithm of breast tumor proliferation level proposed in this study is shown in Fig. 2. The use of image segmentation techniques is required to extract cells in both the training and application stages. The purpose of extracting cells during the training phase is to add labels to make samples, in which the positive and negative cells need to be distinguished, and the cells cannot be over-divided to prevent the over-fitting of CNN. The cells are extracted at the application stage for subsequent cell sorting and counting. As shown in Fig. 1, the staining intensity of the cells in the sectioned microscopic image is evenly distributed between blue and dark brown, and abnormal proliferation of tumor cells leads to increased adhesion between cells. In order to extract different types of cells, we combine two cell segmentation

techniques to treat breast tumor cell pathological images.

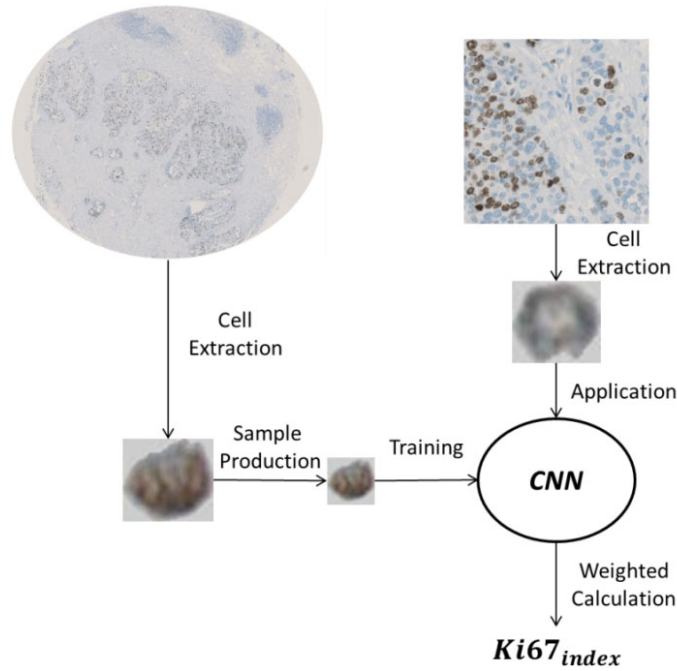


Figure 2: Image recognition in CNN

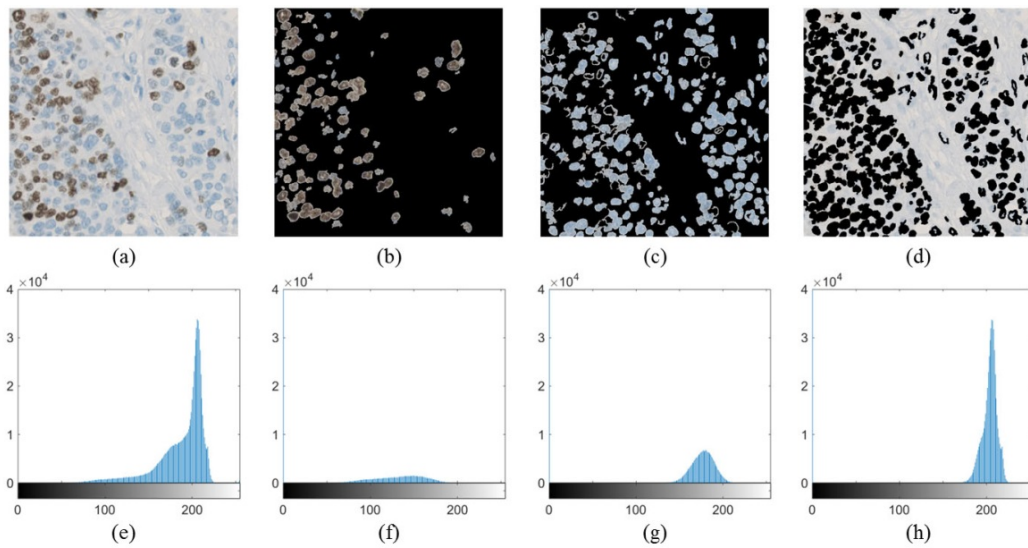


Figure 3: Multi-channel threshold segmentation; (a) original image, (b) positive cell set, (c) negative cell set, (d) background, (e) gray histogram of original image, (f) gray histogram of positive cell set, (g) gray histogram of negative cell set, (h) gray histogram of background

First of all, this study uses a multi-channel threshold segmentation method. The cell and background were separated by thresholding the I-channel image in the HSI model, and the negative and positive cells were differentiated by the threshold segmentation of the B-channel image in the RGB model, thereby dividing the original image into positive and negative cell sets and backgrounds. In three parts, the segmentation results are shown in Fig. 3. Figs. 3(a)-3(d) are the original image, positive cell (P cell) set, negative cell (N cell) set and background; Figs. 3(e)-3(h) shows the gray histogram. It can be seen from Fig. 3 that the gray value of the positive cells is uniformly distributed between 60 and 190, and the gray value of the negative cells is between 130 and 220 and is concentrated in the range of 150 to 200. Therefore, the division of the negative cells and the positive cells in the pathological section is not absolute, and both of them are distributed in the gray-scale range of 130 to 190.

Then, the segmented positive and negative cell sets were further divided using a watershed algorithm to extract positive cells and negative cells. The watershed represents the local maxima of the input image and the method has a good response to weak edges [Patras, Hendriks and Lagendijk (2001)]. The watershed method is able to generate continuous boundaries of cell division and fast calculation, but is likely to cause excessive segmentation. Correcting the gradient image by iterating the foreground marker yields [Koyuncu, Akhan, Ersahin et al. (2016)] a satisfactory segmentation result, as shown in Fig. 4. Among them, positive cells are in the orange region and negative cells are in the blue region. In the cell extraction process during the training phase, the lymphocyte and non-cellular substances are grouped together to reduce the interference to the counting during the application phase of the convolutional neural network.

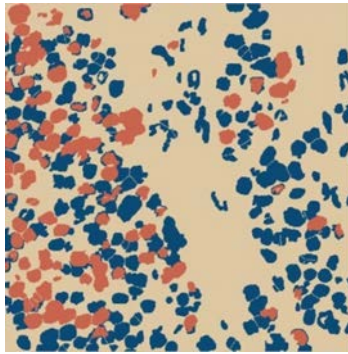


Figure 4: Watershed segmentation

In addition, the segmentation results of Fig. 4 show that most single cells can be extracted, but some cells will adhere into a cell mass. The cell masses in the adhesive state mainly have three forms: Two-cell adhesions, three-cell bulk adhesions, and three-cell chain adhesions. In this study, these three types of adhesions are counted as one class separately, and the convolutional neural network is used to extract high-dimensional features to improve the robustness of the algorithm. Individual cells and adherent cell masses were kept in aspect ratios, placed in a 28×28 image as samples, and then be tagged. Take the positive cells as an example, independent cells are considered as a class and three adhesion states are considered as three classes. Thus, positive cells and negative cells are provided with 8 different types of

labels. In order to improve the recognition accuracy, another type of invalid cell is added. Fig. 5 shows all 9 types of samples obtained by target extraction.

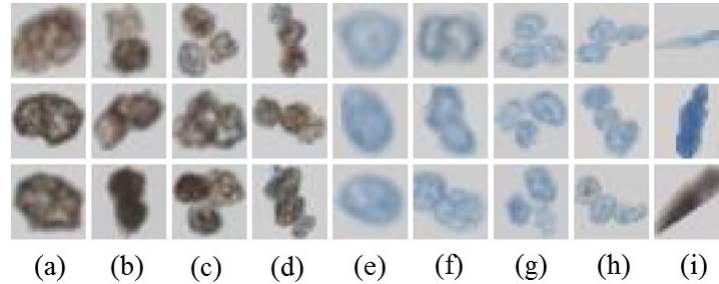


Figure 5: Nine types of samples; (a) positive single cells, (b) positive two-cell adhesions, (c) positive three-cell bulk adhesions, (d) positive three-cell chain adhesions, (e) negative single cells, (f) negative two-cell adhesions, (g) negative three-cell bulk adhesions, (h) positive three-cell chain adhesions, (i) invalid cells

3.3 Network structure

The convolutional neural network used in this study consists of a six-layer network structure, including two convolutional layers C1 and C2, two pooling layers P1 and P2, one dropout layer D, and one fully connected layer F. The specific structure is shown in Fig. 6. In order to provide the network with better generalization ability, the image block is preprocessed by graying and normalization, and pictures with a size of 28×28 are then input into the network as training samples. In the convolution layer C1, the input blocks are convoluted using six 5×5 convolution kernels, and six feature maps with the size of 24×24 are obtained. In the pooling layer P1, six 12×12 feature maps are obtained by sampling the feature map after the upper layer convolution using a maximum pool size of 2×2 . In the convolutional layer C2, twelve 5×5 convolution kernels are used to convolve the feature maps after the upper sampling, and 12 feature maps having a size of 8×8 are obtained. After the pooling layer C2 and the dropout layer D, we further reduce the feature number and adopt a full connection method at the output layer. Although the feature maps extracted through the two convolution and pooling operations are reduced in size, they can still guarantee the expressiveness of the features.

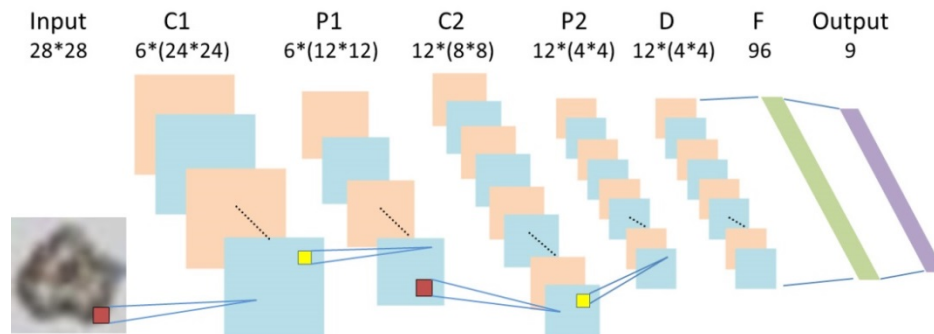
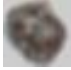



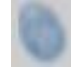






Figure 6: The structure of convolutional neural network

4 Results and discussion

The experimental data comes from <http://pan.baidu.com/s/1mhGmS0S>. There are 11 microscopic section images of mammary gland tumors, each of which contained 10,000 cells to 20,000 cells. We collected 100 pictures within a fixed-size field of view from these Slides. One example is shown in Fig. 1, which contained about 400 cells. In the process of building sample's database, the cell's segmentation approach proposed in this study is not always successful to all positive and negative cells, especial when their proportion is severely imbalanced. However, we can choose the properly segmented cells and labelled them artificially to overcome this problem. Then, the sample's database of breast cancer Ki-67 immunohistochemistry is established under the guidance of clinic doctors. In order to improve the robustness and generalization of convolutional neural networks, the dataset is augmented by adding Gaussian noise, flip and rotation transformations to the samples. Tab. 1 shows the legends for each type of samples and the number of samples before and after data augmentation (DA). Among them, raw data of the 3rd, 4th, 7th, and 8th types are less, and the amount of data reach the same order of magnitude as other types after data augmentation. The convolutional neural network was eventually trained with 40,000 training samples and 20,000 test samples.

Table 1: Sample distribution

Type	1	2	3	4	5	6	7	8	9
Legend									
Sample Size Before DA	1200	900	200	200	1200	900	200	200	900
Sample Size After DA	9600	7200	4800	4800	9600	7200	4800	4800	7200

When training the network, the number of samples extracted at each iteration is set to 100, and stop the iteration when the classification error is less than 8%. In order to verify the classification ability of the trained convolutional neural network, this study tested Fig. 1 with a size of 900×900. According to a doctor, it contains 107 positive cells and 347 negative cells. The classified number of nine types of samples is shown in Tab. 2, in which T_i ($i=1, 2, \dots, 9$) is the statistic results by the doctor and P_j ($j=1, 2, \dots, 9$) in the predicted results by CNN.

By comparing the accuracy of various classifications, it was found that the classification errors of several types (such as T_1 , T_2 , T_5 , and T_6) with more raw samples were all below 10%. The classification accuracy of trained CNN was

$$accuracy = \sum_1^9 \left(\frac{\sum \{n_{(t,p)} | t = T_i\}}{\sum \{n_{(t,p)} | t = t\}} * accuracy_i \right) = 93.53\% \quad (6)$$

where $accuracy_i$ denotes the classification accuracy of class T_i , and $n_{(t,p)}$ denotes the

sample number with true classification t and prediction classifier p . Tumor proliferation levels were calculated based on the classification results in Tab. 2.

Table 2: The number of nine types of cell classified by doctor and CNN

	Prediction									Accuracy (%)
	P_1	P_2	P_3	P_4	P_5	P_6	P_7	P_8	P_9	
T_1	37	2	-	-	1	-	-	-	1	90.24
T_2	1	20	-	-	-	-	-	-	-	95.24
T_3	-	-	4	-	-	-	-	-	1	80
T_4	-	-	-	3	-	-	-	-	-	100
Truth T_5	2	-	-	-	154	6	-	1	4	92.22
T_6	-	-	-	-	-	65	-	2	2	94.20
T_7	-	-	1	-	-	-	5	-	-	83.33
T_8	-	-	-	-	-	1	-	7	-	87.5
T_9	2	-	-	-	4	1	-	-	82	92.13

$$N_{pos_pred} = \sum_{p=P1} n_{(t,p)} + 2 * \sum_{p=P2} n_{(t,p)} + 3 * \sum_{p=P3|P4} n_{(t,p)} \quad (7)$$

$$N_{pred_neg} = \sum_{p=P5} n_{(t,p)} + 2 * \sum_{p=P6} n_{(t,p)} + 3 * \sum_{p=P7|P8} n_{(t,p)} \quad (8)$$

$$N_{true_pos} = \sum_{t=T1} n_{(t,p)} + 2 * \sum_{t=T2} n_{(t,p)} + 3 * \sum_{t=T3|T4} n_{(t,p)} \quad (9)$$

$$N_{true_pos} = \sum_{t=T5} n_{(t,p)} + 2 * \sum_{t=T6} n_{(t,p)} + 3 * \sum_{t=T7|T8} n_{(t,p)} \quad (10)$$

$$Ki67_{index_pre} = \frac{N_{pos_pred}}{N_{pos_pred} + N_{pred_neg}} = 0.2391 \quad (11)$$

$$Ki67_{index_tru} = \frac{N_{true_pos}}{N_{true_pos} + N_{true_pos}} = 0.2356 \quad (12)$$

N_{pos_pred} and N_{pred_neg} respectively represents the predicted number of positive breast tumor cells and negative tumor cells, N_{true_pos} and N_{true_pos} each represents the true number of positive breast tumor cells and negative tumor cells. For the test image, the relative error of tumor proliferation levels can be calculated.

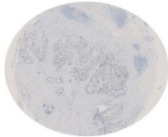

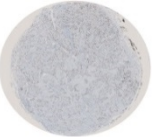
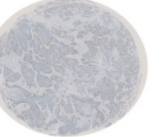
$$\delta = \frac{Ki67_{index_pre} - Ki67_{index_tru}}{Ki67_{index_tru}} = 1.49\% \quad (13)$$

The results meet the requirement that the relative error be less than 10%.

In order to further verify the reliability of the breast cancer proliferation level recognition

algorithm based on the convolutional neural network, four slides reflecting different degrees of malignancy were selected from the breast tumor pathological database for identification, and five independent images with more than 400 cells were taken from each slide within a fixed-size field of view. In the test of each slide, the number of cells is more than 2,000. The statistical results are shown in Tab. 3.

Table 3: Quantitative analysis of the recognition algorithm

Slide				
Mean of Proliferation Level	9.16%	19.55%	22.32%	39.79%
Mean of Accuracy	90.77%	93.80%	90.12%	92.62%
Variance of Accuracy	3.12%	2.96%	4.05%	3.64%
Mean of Relative Error	2.71%	1.76%	2.93%	1.85%

The mean relative error generated when calculating the proliferation level for the selected 4 slides was less than 5%; meanwhile, the mean value of the classification error when the tumor cells or cell blocks were classified in each figure by the convolutional neural network was lower than 10%. This result shows the effectiveness of the proposed method for the automatic identification of mammary tumor proliferation. In future studies, the number of samples of tumor cells will be increased to improve the classification accuracy of the network.

5 Conclusion

In order to meet the requirements of high accuracy and speed in the quantitative analysis of tumor cells in pathological section images, we propose a method of automatic recognition of tumor proliferation level based on convolutional neural networks. In this study, a variety of image segmentation methods are adopted to accomplish breast cancer cell extraction and sample's database establishment. The convolutional neural network with six layer network structure is built to learn the characteristics of breast cancer cells for identifying and classifying mammary gland tumor cells with different differentiation capabilities. The experimental results show that the convolutional neural network proposed in this study can accurately separate positive and negative cells of different forms, which has values in clinical application in the identification and diagnosis of early tumors.

Acknowledgements: This study was supported by the National Natural Science Foundation of China (Grant No. 61171059).

References

- Atanassov, B. S.; Mohan, R. D.; Lan, X.; Kuang, X.; Lu, Y. et al.** (2016): ATXN7L3 and ENY2 coordinate activity of multiple H2B deubiquitinases important for cellular proliferation and tumor growth. *Molecular Cell*, vol. 62, no. 4, pp. 558-571.
- Bottou, L.** (2010): Large-scale machine learning with stochastic gradient descent. *Proceedings of COMPSTAT'2010*, pp. 177-186.
- Dowsett, M.; Nielsen, T. O.; A'Hern, R.; Bartlett, J.; Coombes, R. C. et al.** (2011): Assessment of Ki-67 in breast cancer: recommendations from the international Ki-67 in breast cancer working group. *Journal of the National Cancer Institute*, vol. 103, no. 22, pp. 1656-1664.
- Fan, D.; Wei, L.; Cao, M.** (2016): Extraction of target region in lung immunohistochemical image based on artificial neural network. *Multimedia Tools and Applications*, vol. 75, no. 19, pp. 12227-12244.
- Focke, C. M.; van Diest, P. J.; Decker, T.** (2016): St Gallen 2015 subtyping of luminal breast cancers: impact of different Ki-67-based proliferation assessment methods. *Breast Cancer Research and Treatment*, vol. 159, no. 2, pp. 257-263.
- Friedman, A.; Kim, Y.** (2010): Tumor cells proliferation and migration under the influence of their microenvironment. *BIOMAT 2009*. World Scientific.
- Huang, G.; Chen, S.; Wang, D.; Wang, R.; Lin, L. et al.** (2016): High Ki-67 expression has prognostic value in surgically-resected T3 gastric adenocarcinoma. *Clinical Laboratory*, vol. 62, no. 1-2, pp. 141-153.
- Ikemura, M.; Shibahara, J.; Mukasa, A.; Takayanagi, S.; Aihara, K. et al.** (2016): Utility of ATRX immunohistochemistry in diagnosis of adult diffuse gliomas. *Histopathology*, vol. 69, no. 2, pp. 260-267.
- Juríková, M.; Danihel, E.; Polák, Š.; Varga, I.** (2016): Ki-67, PCNA, and MCM proteins: Markers of proliferation in the diagnosis of breast cancer. *Acta Histochemica*, vol. 118, no. 5, pp. 544-552.
- Ko, C. C.; Chen, Y. R.; Lin, W. Y.** (2016): Improving the evaluation accuracies of histopathologic grade and ki-67 immunohistochemistry expression of breast carcinoma using computer image processing (II). *International Computer Symposium*, pp. 410-414.
- Koyuncu, C. F.; Akhan, E.; Ersahin, T.; Cetin-Atalay, R.; Gunduz-Demir, C.** (2016): Iterative h-minima-based marker-controlled watershed for cell nucleus segmentation. *Cytometry Part A*, vol. 89, no. 4, pp. 338-349.
- Krizhevsky, A.; Sutskever, I.; Hinton, G. E.** (2012): Imagenet classification with deep convolutional neural networks. *Advances in neural information processing systems*, pp. 1097-1105.
- LeCun, Y.; Bottou, L.; Bengio, Y.; Haffner, P.** (1998): Gradient-based learning applied to document recognition. *Proceedings of the IEEE*, vol. 86, no. 11, pp. 2278-2324.
- Li, F.; Tran, L.; Thung, K. H.; Ji, S.; Shen, D. et al.** (2014): Robust deep learning for improved classification of AD/MCI patients. *International Workshop on Machine Learning in Medical Imaging*, pp. 240-247.

- Li, Y.; Hao, Z.; Lei, H.** (2016): Survey of convolutional neural network. *Journal of Computer Applications*, vol. 36, no. 9, pp. 2508-2515.
- Patras, I.; Hendriks, E. A.; Lagendijk, R. L.** (2001): Video segmentation by MAP labeling of watershed segments. *IEEE Transactions on Pattern Analysis and Machine Intelligence*, vol. 23, no. 3, pp. 326-332.
- Salomon, G.; Köllerman, J.; Thederan, I.; Chun, F. K.; Budäus, L. et al.** (2008): Evaluation of prostate cancer detection with ultrasound real-time elastography: A comparison with step section pathological analysis after radical prostatectomy. *European Urology*, vol. 54, no. 6, pp. 1354-1362.
- Shete, P. G.; Kharate, G. K.** (2015): Evaluation of immunohistochemistry (IHC) biomarkers in breast cancer using digital image processing. *Journal of Life Sciences and Technologies*, vol. 3, no. 2.
- Shi, P.; Zhong, J.; Hong, J.; Huang, R.; Wang, K. et al.** (2016): Automated ki-67 quantification of immunohistochemical staining image of human nasopharyngeal carcinoma xenografts. *Scientific Reports*, vol. 6.
- Shui, R.; Yu, B.; Bi, R.; Yang, F.; Yang, W.** (2016): An interobserver reproducibility analysis of Ki-67 visual assessment in breast cancer. *Pathology*, vol. 48, no. 5, pp. S155-S156.
- Soos, B. G.; Rak, A.; Veres, J.; Cserey, G.** (2008): GPU powered CNN simulator (SIMCNN) with graphical flow based programmability. *International Workshop on Cellular Neural Network*, vol. 2018, pp. 163-168.
- Van Eycke, Y. R.; Allard, J.; Salmon, I.; Debeir, O.; Decaestecker, C.** (2017): Image processing in digital pathology: An opportunity to solve inter-batch variability of immunohistochemical staining. *Scientific Reports*, vol. 7.
- Yang, Z.; Tang, L. H.; Klimstra, D. S.** (2011): Effect of tumor heterogeneity on the assessment of Ki-67 labeling index in well-differentiated neuroendocrine tumors metastatic to the liver: implications for prognostic stratification. *American Journal of Surgical Pathology*, vol. 35, no. 6, pp. 853-860.
- Zbontar, J.; LeCun, Y.** (2016): Stereo matching by training a convolutional neural network to compare image patches. *Journal of Machine Learning Research*, vol. 17, pp. 1-32.